

Generalizable Deepfake Detection via Effective Local-Global Feature Extraction

Jiazhen Yan¹, Ziqiang Li¹, Ziwen He¹ and Zhangjie Fu^{1*}

¹ Engineering Research Center of Digital Forensics, Ministry of Education, Nanjing University of Information Science and Technology

247918horizon@gmail.com, iceli@mail.ustc.edu.cn, {ziwen.he, fzj}@nuist.edu.cn

Abstract

The rapid advancement of GANs and diffusion models has led to the generation of increasingly realistic fake images, posing significant hidden dangers and threats to society. Consequently, deepfake detection has become a pressing issue in today's world. While some existing methods focus on forgery features from either a local or global perspective, they often overlook the complementary nature of these features. Other approaches attempt to incorporate both local and global features but rely on simplistic strategies, such as cropping, which fail to capture the intricate relationships between local features. To address these limitations, we propose a novel method that effectively combines local spatial-frequency domain features with global frequency domain information, capturing detailed and holistic forgery traces. Specifically, our method uses Discrete Wavelet Transform (DWT) and sliding windows to tile forged features and leverages attention mechanisms to extract local spatial-frequency domain information. Simultaneously, the phase component of the Fast Fourier Transform (FFT) is integrated with attention mechanisms to extract global frequency domain information, complementing the local features and ensuring the integrity of forgery detection. Comprehensive evaluations on open-world datasets generated by **34 distinct generative models** demonstrate a significant improvement of **2.9%** over existing state-of-the-art methods.

1 Introduction

With the rapid advancement of deep learning, generative models such as GANs and diffusion models have revolutionized content creation, finding widespread applications across industries including entertainment and media. However, this progress has also introduced significant challenges. The increasing sophistication of deepfake technology has allowed the generation of highly realistic fake images and videos, making them increasingly difficult to detect and posing serious risks to societal trust, individual privacy, and security.

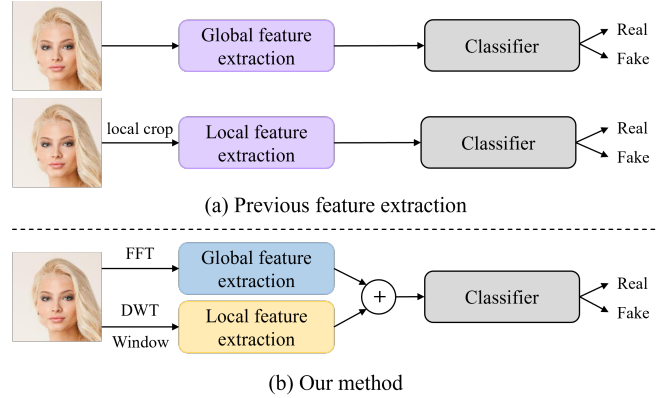


Figure 1: **Comparison with Previous Methods.** Previous methods often extract only local information or global information to detect artifact information. However, these methods are not enough to fully capture effective artifact information. Recent methods also combine local and global information to detect forged images, but they only extract local information through simple cropping, destroying the relationship between local information. Compared with them, our method uses DWT and sliding window tiling to reasonably and effectively extract local time-frequency information, and combines the phase part of FFT to extract global frequency domain information.

In response, various deepfake detection mechanisms have been conceived. Early methods primarily focused on analyzing image features, such as texture, color, and lighting [Yu *et al.*, 2020; Liu *et al.*, 2020], to identify forgery traces. However, these approaches were often limited to training and testing within a single domain, overlooking the critical issue of cross-domain generalization. In real-world scenarios, it is essential for detection models to effectively generalize to unseen deepfake sources, including those involving unfamiliar generative models or novel categories.

In recent years, substantial efforts have been devoted to forgery detection, particularly to identifying deepfake sources that are challenging to detect in real-world scenarios, as illustrated in Figure 1 (a). To enhance generalization performance, some studies emphasize fine-grained features, such as local artifacts [Haliassos *et al.*, 2021; Chen *et al.*, 2022] and the relationships between pixel points [Chen *et al.*, 2021; Tan *et al.*, 2024b]. Others focus on global artifact traces, including global spatial information [Tan *et al.*, 2023; Ojha

al., 2023] and frequency-domain features [Tan *et al.*, 2024a]. However, prioritizing either local or global information in isolation may result in the loss of complementary details, thereby limiting generalization capabilities. To address this limitation, some methods integrate both local and global features. For example, [Chen and Yang, 2020] extract local features through clipping in the spatial domain while leveraging global features in the frequency space. Similarly, [Wu *et al.*, 2024] employ a local attention module and facilitates interaction with features from distant adjacent PPG graphs to capture local and global information, respectively. However, these approaches often rely on coarse image block segmentation for local feature extraction, which can lead to forced separation and loss of relevant feature relationships.

Accordingly, we propose a simple yet efficient feature extractor to capture global frequency domain and local spatial-frequency domain information, as illustrated in Figure 1 (b), which is plug-and-play and can be integrated with any CNN classifier. Specifically, our method introduces two key modules, DWT-Based Local Spatial-Frequency Domain Feature Capture Block (LoSFB) and FFT-Based Global Frequency Domain Feature Capture Block (GloFB), both using the Window Attention Block as the feature extractor. After performing the DWT, we concatenate features from four different frequency bands, each with dimensions $h \times w$. Then a 2×2 sliding window is applied to extract the tiled features from each frequency band. Finally, the features within the window are tiled again, resulting in new features with dimensions $4 \times (h \times w)$. At this time, when we extract the 4×4 window features, they not only obtain features in four frequency domains, but also retain the local spatial-frequency information within the window, greatly improving the effect of artifact detection. Additionally, we incorporate the phase information from the FFT as a complement to the DWT, enabling the extraction of global frequency domain information. This helps guide the network to effectively learn global artifact patterns and identify more comprehensive traces of forgery. To fully assess the generalizability of our method, we evaluate it on large image datasets generated by 34 distinct models¹. Comprehensive experiments demonstrate that our method generalizes well across diverse and unseen sources, demonstrating a significant improvement over state-of-the-art methods by 2.9%. Our paper makes the following contributions:

- We propose a plug-and-play feature extractor that seamlessly integrates local spatial-frequency and global frequency-domain information. This method can be effortlessly incorporated into any CNN classifier and effectively improves the model’s generalization capability.
- We use sliding window interpretability to extract local spatial frequency information, and creatively use only phase spectrum to obtain global features to capture

¹ProGAN, StyleGAN, StyleGAN2, BigGAN, CycleGAN, StarGAN, GauGAN, Deepfake, WFIR, SAN, AttGAN, BEGAN, CramerGAN, InfoMaxGAN, MMDGAN, ReIGAN, S3GAN, SNGAN, STGAN, ADM, DDPM, IDDP, LDM, PNDM, VQD-diffusion, Stable-Diffusion v1, Stable-Diffusion v2, DALLE, Glide, Midjourney, Stable-Diffusion v1.4, Stable-Diffusion v1.5, Wukong, DALLE-2

broader forgery artifacts.

- Our experiments validate the effectiveness of the proposed method, which exhibits strong generalization across image detection tasks involving 34 different generation models. The method achieves a notable 2.9% improvement over state-of-the-art approaches, highlighting its superiority and robustness.

2 Related Work

In this section, we present a concise review of deepfake detection methods, mainly dividing them into three main groups: deepfake detection based on local information, deepfake detection based on global information, and deepfake detection based on local and global information fusion.

2.1 Deepfake Detection Based on Local Information

Early researches on deepfake detection often focus on specific facial regions, such as the eyes and lips, to identify forgery traces [Haliassos *et al.*, 2021; Chen *et al.*, 2022]. However, as forgery techniques have advanced, these simple traces have been increasingly refined and obscured, rendering biometric-based detection methods insufficient for identifying sophisticated forged images. Experiments have shown that forgery traces are often embedded in fine-grained details, prompting a shift in focus toward extracting local artifact information. For instance, [Chai *et al.*, 2020] use limited receptive fields to capture local features, while [Zhao *et al.*, 2021] employ multiple spatial attention heads to enhance the network’s focus on distinct local regions. Other studies analyze forgery traces by examining relationships between local pixels. [Chen *et al.*, 2021] propose learning the similarity of local regions for a fine-grained assessment of patch similarity across scales, and [Tan *et al.*, 2024b] improve forgery detection generalization by identifying upsampling artifacts in nearby pixel grids. While capturing local artifact details, these methods overlook the fact that the overall image may still contain forged features, which are essential for generalization.

2.2 Deepfake Detection Based on Global Information

Early studies leveraged spatial information from generated images to detect fake content. For example, [Yu *et al.*, 2020; Liu *et al.*, 2020] distinguish real and fake images using global information, such as color space and global texture. Some studies [Yu *et al.*, 2019] use GANs to generate global fingerprint information that may assist in detection. Additionally, [Tan *et al.*, 2023] and [Ojha *et al.*, 2023] extract artifact representations using global feature maps and global feature gradients, respectively. Moreover, since GAN-generated images often rely on upsampling operations that introduce artifacts at the frequency domain level, several studies have explored forgery detection in the frequency domain. For instance, [Tan *et al.*, 2024a] use FFT to extract global high-frequency information, uncovering more refined forgery features. While these methods capture sufficient global artifact information, they overlook the fact that effective artifact features often reside in subtle, localized regions. The neglect of local artifact

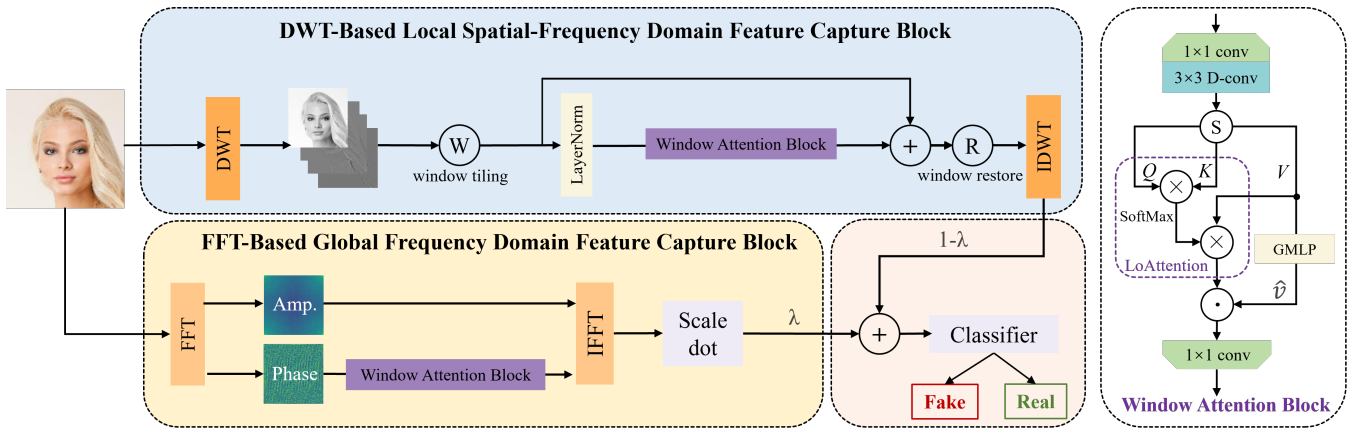


Figure 2: **Architecture of Our Method for Generalizable Deepfake Detection.** In order to capture more comprehensive and reasonable forgery features, we use LoSFB and GloFB to capture local and global information, respectively. Specifically, we use DWT and sliding window tiling to construct local spatial-frequency features, and only use the phase part of FFT to construct global frequency domain features. Both of them use Window Attention Block to extract features. In addition, in order to weaken the information weight of global features, we add hyperparameters λ to the global features when merging the two types of features. The final extracted features are passed into a classifier.

information can significantly impair the generalization capabilities of forgery detection.

2.3 Deepfake Detection Based on Local and Global Information Fusion

Whether relying on global or local information alone, these methods detect forgery using only a single category of features, overlooking the significant information gain that arises from combining complementary features at different levels. [Chen and Yang, 2020] capture local features through spatial domain cropping and global features in the frequency domain. [Xue *et al.*, 2023] employ separate branches for local area feature extraction and global feature extraction, using the latter to obtain residual features. [Wu *et al.*, 2024] introduce a local attention module that interacts with distant neighboring PPG graphs to gather both local and global information. While these studies incorporate both global and local information, their approach to processing local information is limited by artificial segmentation of the face into regions, which leads to the loss of important forged details.

3 Main Backbone

The overall structure of our method is shown in Figure 2. Inspired by [Mao *et al.*, 2024], we propose an efficient local-global feature extraction framework designed to capture both global and local information. Specifically, the framework consists of two main branches: LoSFB and GloFB. Both branches utilize the Window Attention Block to extract the most relevant features, which are then fused and passed to the classifier for final classification. Notably, our approach is compatible with any classifier, allowing us to focus primarily on the feature extraction process.

3.1 Window Attention Block

The Window Attention Block (WAttention) consists of two main components: (i) the Local Attention Block (LoAttention) and (ii) the Global Window MLP Layer (GMLP). Before

feeding the features into LoAttention and GMLP, we preprocess them to enhance their representational quality. A 1×1 convolution layer is applied to extract cross-channel features, following by a 3×3 depthwise separable convolution to better capture the local features within each channel. The resulting convolved features are denoted as $X_{in} \in \mathbb{R}^{B \times C \times H \times W}$.

LoAttention. Unlike traditional attention mechanisms, which are typically designed to capture global information, we employ a sliding window approach that divides the features into windows of size $b \times b$. By restricting the attention module to these local windows, the focus shifts to effectively extracting local features. The features are then divided into $Q, K, V \in \mathbb{R}^{S \times C \times N}$, where $S = B \times \frac{H}{b} \times \frac{W}{b}$ and $N = b \times b$, as required by the attention module. Since the attention operates locally within each window, the features within window i are represented as $Q_i, K_i, V_i \in \mathbb{R}^{C \times N}$. These localized features are fed into the attention module for computation:

$$A_i = \text{Attention}(Q_i, K_i, V_i) = \text{SoftMax}(Q_i K_i^T) V_i. \quad (1)$$

The results of all window attention operations can be expressed as $A = \{A_1, A_2, \dots, A_S\} \in \mathbb{R}^{S \times C \times N}$.

GMLP. To preserve global correlations while capturing fine-grained features, we integrate a global MLP within each window. This aims to address the limitations of local windows in modeling global relationships, ensuring a seamless fusion of local details and global context. Specifically, we reuse the value V_i from LoAttention and process it through the global MLP, applying a nonlinear transformation to enhance its representational capacity. The result \hat{V}_i is formally expressed as:

$$\text{GMLP}(V_i) = G(\text{Linear}(V_i)), \quad (2)$$

where $G(\cdot)$ denotes the GELU function. The GMLP recombines and redistributes the local window information, enabling the mixing of local frequency domain features and enhancing the learning of global features.

After combining the outputs from LoAttention and GMLP via a dot product, we use the inverse window operation to restore the feature to its original size $B \times C \times H \times W$, followed

by a convolution to map the features back to the original feature dimensions. The final output of the WAttention can be expressed as:

$$X_W = \text{conv}\left(\sum_{i=1}^s \text{Attention}(Q_i, K_i, V_i) \cdot \sum_{i=1}^s G(\text{Linear}(V_i))\right). \quad (3)$$

3.2 DWT-Based Local Spatial-Frequency Domain Feature Capture Block

Previous methods often leverage the Fast Fourier Transform (FFT) or Discrete Cosine Transform (DCT) to capture relationships between adjacent nodes in the frequency domain. However, these approaches can lead to the loss of positional information, which is crucial for extracting detailed features. To overcome this limitation, we utilize the Discrete Wavelet Transform (DWT), which decomposes the image into the spatial-frequency domain, represented as:

$$\text{DWT}(I) = \{I_{LL}, I_{LH}, I_{HL}, I_{HH}\}, \quad (4)$$

where $I_{LL}, I_{LH}, I_{HL}, I_{HH} \in \mathbb{R}^{C \times \frac{H}{2} \times \frac{W}{2}}$ represent the low-frequency component of the input and the high-frequency components in the vertical, horizontal, and diagonal directions, respectively. To obtain more comprehensive information, we fuse the data from the four frequency domains, resulting in new input features $\hat{I} \in \mathbb{R}^{4 \times C \times \frac{H}{2} \times \frac{W}{2}}$. As illustrated in Figure 3, to extract detailed features, we divide each channel’s features into 2×2 windows, with each window capturing localized spatial-frequency information within its respective frequency band. Each window is treated as a small square and tiled into rows within each band. This arrangement ensures that features within the 2×2 windows are preserved in a structured format. Then we tile the features in the window here by rows. At this time, the features from each frequency band are tiled into one row in a specific manner, such that the four adjacent feature values correspond to the 2×2 window from the original image. Additionally, as shown in Figure 3, we integrate features from all frequency bands to generate new input features $\hat{I}_{\text{input}} \in \mathbb{R}^{C \times 4 \times \frac{H}{4} \times \frac{W}{4}}$. To further enhance the network’s performance, we apply LayerNorm [Lei Ba *et al.*, 2016], which ensures that the input data remains within a stable range, reduces dependency on initialization, and improves the stability of model training.

The feature \hat{I}_{input} is then fed into WAttention with a sliding window size set to $b = 4$. As depicted in Figure 3, within each 4×4 window, the representation includes not only the four adjacent feature values from the original image but also the feature information across four distinct frequency bands. This configuration provides WAttention with comprehensive and fine-grained spatial-frequency domain information, enabling more detailed feature extraction. Following this process, we apply the IDWT to reconstruct the features back into spatial domain representations, denoted as $\hat{I}_{\text{DWT.output}}$.

3.3 FFT-Based Global Frequency Domain Feature Capture Block

Although artifact information is often concentrated in finer details, forged features can also be embedded in the global information of an image, remaining imperceptible to the naked

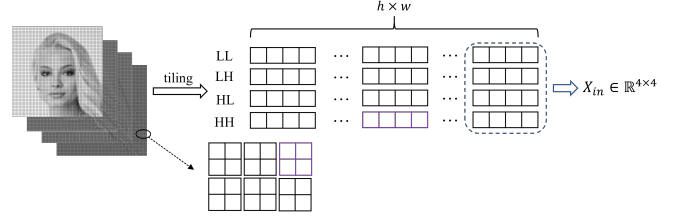


Figure 3: After DWT, sliding window tiling is used to tile the features of each channel into a shape of $4 \times (h \times w)$. In the subsequent LoAttention module, 4×4 features are extracted as shown in the blue box, which not only contains local spatial frequency information, but also contains all different frequency band features.

eye. While DWT and sliding window tiling are effective for extracting local features, we also use FFT capture global frequency domain information from a complementary perspective. In this module, FFT is employed to transform the image into the frequency domain at the pixel level, enabling the extraction of global frequency domain features. Inspired by [Zhao *et al.*, 2024], we recognize that amplitude primarily reflects properties such as color and brightness, while phase encodes finer details, including potential artifacts. Based on this insight, we focus on extracting the phase features as input to WAttention, setting the window size to $b = 8$. The amplitude remains unmodified during this process. After training the phase features, we use IFFT to recombine them with the original amplitude, transforming the features back into the spatial domain. The resulting features are denoted as $\hat{I}_{\text{FFT.output}}$.

Finally, we set a hyperparameter λ to minimize the impact of global information extraction. The final feature is:

$$\hat{X}_{\text{output}} = (1 - \lambda) * \hat{I}_{\text{DWT.output}} + \lambda * \hat{I}_{\text{FFT.output}}. \quad (5)$$

4 Experiments

To verify the excellent deepfake detection performance of our method, we follow the paradigms of [Ojha *et al.*, 2023] and [Wang *et al.*, 2020].

4.1 Dataset

Training set. To ensure a consistent basis for comparison, we use the training set of ForenSynths[Wang *et al.*, 2020]. The training set consists of 20 different categories, each containing 18,000 synthetic images generated using ProGAN, and an equal number of real images from the LSUN dataset. Following the paradigms of [Ojha *et al.*, 2023], we adopt specific 4-class training settings, denoted as (car, cat, chair, horse).

Testing set. In order to comprehensively compare the effectiveness of our proposed method, we select different GAN and diffusion datasets for testing, which contain a wide range of real-world images.

- ForenSynths: The test set comprises 10 subsets, including: ProGAN [Karras, 2017], StyleGAN [Karras, 2019], StyleGAN2 [Karras *et al.*, 2020], BigGAN [Brock, 2018], CycleGAN [Zhu *et al.*, 2017], StarGAN [Choi *et al.*, 2018], GauGAN [Park *et al.*, 2019], Deepfake [Rossler *et al.*, 2019], WFIR and SAN [Dai *et al.*, 2019].

- GANGen-Detection [Tan *et al.*, 2024a]: To evaluate more realistic scenarios, we extend our evaluation using 9 additional GAN-generated images. There are 4K test images for each model, with equal numbers of real and fake images.
- DiffusionForensics [Wang *et al.*, 2023]: To expand the testing scope, we adopt the diffusions dataset of DIRE [Wang *et al.*, 2023] for evaluation, including ADM [Dhariwal and Nichol, 2021], DDPM [Ho *et al.*, 2020], IDDPM [Nichol and Dhariwal, 2021], LDM [Rombach *et al.*, 2022], PNDM [Liu *et al.*, 2022], VQ-Diffusion [Gu *et al.*, 2022], Stable Diffusion v1 [Rombach *et al.*, 2022], Stable Diffusion v2 [Rombach *et al.*, 2022]. The real images are sampled from LSUN [Yu *et al.*, 2015] and ImageNet [Russakovsky *et al.*, 2015] datasets.
- UniversalFakeDetect [Ojha *et al.*, 2023]: This test set contains images generated from Glide [Nichol *et al.*, 2021], DALL-Emini [Ramesh *et al.*, 2021], LDM [Rombach *et al.*, 2022]. It adopts images of LAION [Schuhmann *et al.*, 2021] and ImageNet [Russakovsky *et al.*, 2015] datasets as the real data.
- AIGCDetectBenchmark [Zhu *et al.*, 2024]: This dataset mainly adopts diffusion model to generate images, and is generated using more realistic advanced methods, including Midjourney, SDv1.4, SDv1.5 [Rombach *et al.*, 2022], ADM [Dhariwal and Nichol, 2021], GLIDE [Nichol *et al.*, 2021], Wukong, VQDM [Gu *et al.*, 2022], which is a huge challenge for deepfake detection.

4.2 Implementation Details

We design a lightweight CNN network using convolutional layers and Resnet network as classifiers. The network is trained using the Adam optimizer [Kingma, 2014] with a learning rate of 2×10^{-4} . The batchsize is set to 128, and we train the network for 90 epochs. We also use a learning rate decay strategy that reduces the learning rate by twenty percent after every ten epochs. What’s more, the hyperparameter λ is set to 0.2. Our approach is implemented using PyTorch on an NVIDIA RTX A6000 GPU. To evaluate the performance of the proposed method, we follow the evaluation metrics used in baselines [Ojha *et al.*, 2023; Tan *et al.*, 2024a], which include average precision score (A.P.) and accuracy (Acc.).

4.3 Quantitative analysis

We compare with the previous methods: CNNDetection [Wang *et al.*, 2020], Patchfor [Chai *et al.*, 2020], F3Net [Qian *et al.*, 2020], FrePGAN [Jeong *et al.*, 2022], GANDetection [Mandelli *et al.*, 2022], LGrad [Tan *et al.*, 2023], Ojha [Ojha *et al.*, 2023], FreqNet [Tan *et al.*, 2024a] and NPR [Tan *et al.*, 2024b]. We conduct two and three sets of experiments on GAN and diffusion respectively.

GAN. As shown in Table 1 and 2, our detection on GAN has achieved good results. Table 1 presents a detailed comparison of detector performance on the test set of ForenSynths [Wang *et al.*, 2020], highlighting higher mean accuracy (Acc.) and comparable mean average precision (A.P.) metrics. For unavailable test results, we use “-” as a placeholder and ex-

clude these values from the average calculations. Our method achieves an average accuracy of 86.9%, which is 1% and 1.7% higher than the latest methods, NPR and FreqNet, underscoring its effectiveness in generalizable deepfake detection. Furthermore, to evaluate cross-GAN-source generalization, we conducted tests on the GANGen-Detection dataset [Tan *et al.*, 2024a], as summarized in Table 2. Our method achieves an impressive average accuracy of 96.5%, significantly outperforming the best-performing baselines, NPR [Tan *et al.*, 2024b] and FreqNet [Tan *et al.*, 2024a], which achieved 94.8% and 94.0%, respectively.

Diffusion. To further evaluate the generalization ability of our method, we train on ProGAN and test on images generated by various diffusion models. The results are presented in Tables 3 and 4. Despite being trained exclusively on ProGAN-generated images, our method demonstrates strong generalization capabilities across diverse diffusion models. Specifically, it achieves mean Accuracy (Acc.) and mean Average Precision (A.P.) of 98.5% and 99.9%, respectively. Compared to NPR and FreqNet, our method improves mean Acc. by 2.9% and 17.8%, respectively. Additionally, on the UniversalFakeDetect dataset [Ojha *et al.*, 2023], our method achieves an average accuracy of 95.0%, representing a notable improvement over existing approaches.

With the rapid advancements in tools like Midjourney and diffusion models, increasingly realistic fake images are being generated, posing significant challenges for deepfake detection. To address this, we conduct additional evaluations on the AIGCDetectBenchmark dataset [Zhu *et al.*, 2024], excluding some subsets of data previously tested. The results, summarized in Table 5, highlight the robustness of our approach. Our method achieves a notable improvement in mean accuracy, outperforming NPR and FreqNet by 3.7% and 7.8%, respectively, and reaching an accuracy of 77.6%.

Conclusion. To comprehensively evaluate the superiority of our method, we test it on the entire GenImage dataset [Zhu *et al.*, 2024] and calculated the average accuracy. The GenImage dataset offers extensive coverage, including content generated by GANs as well as high-definition images from diffusion models. As shown in Table 6, our method achieves optimal detection performance, with an accuracy of 84.7%, significantly surpassing the accuracy of NPR and FreqNet, which are 81.8% and 78.1%, respectively.

4.4 Qualitative Analysis

To further assess the generalization ability of our method, we visualize the logit distributions of NPR and our approach, as shown in Figure 4. This visualization highlights how effectively each trained model distinguishes between real and fake images, showcasing our method’s ability to generalize across diverse fake representations. From the visualization, it is evident that NPR struggles with unseen GAN or diffusion models, showing significant overlap between the logits of real and fake categories, often misclassifying fake images as “real.” In contrast, our method demonstrates superior discrimination, effectively separating “real” and “fake” categories, even when encountering unseen sources.

Method	ProGAN		GauGAN		StyleGAN2		BigGAN		StyleGAN		CycleGAN		StarGAN		Deepfake		WFIR		SAN		Mean	
	Acc.	A.P.	Acc.	A.P.	Acc.	A.P.	Acc.	A.P.	Acc.	A.P.	Acc.	A.P.	Acc.	A.P.	Acc.	A.P.	Acc.	A.P.	Acc.	A.P.	Acc.	A.P.
CNNDetection	91.4	99.4	63.9	92.2	76.4	97.5	52.9	73.3	63.8	91.4	72.7	88.6	63.8	92.2	51.7	62.3	91.7	96.3	48.7	59.5	67.7	85.3
Patchfor	97.8	100.0	57.2	55.4	83.6	98.5	64.7	69.5	82.6	93.1	74.5	87.2	100.0	100.0	85.0	93.2	-	-	75.3	76.3	80.1	85.9
F3Net	99.4	100.0	58.1	56.1	88.0	99.8	65.3	69.9	92.6	99.7	76.4	84.3	100.0	100.0	63.5	78.8	-	-	47.3	46.7	76.7	81.7
FrePGAN	99.0	99.9	60.3	77.1	84.1	98.6	69.2	71.7	80.7	89.6	71.1	74.4	99.9	100.0	70.9	91.9	-	-	-	-	79.3	87.9
LGrad	99.9	100.0	72.4	79.3	96.0	99.9	82.9	90.7	94.8	99.9	85.3	94.0	99.6	100.0	58.0	67.9	60.5	65.1	50.0	51.4	79.9	84.8
Ojha	100.0	100.0	99.7	100.0	75.7	97.8	95.1	99.3	84.4	97.1	98.7	99.8	99.9	99.4	67.4	82.0	64.2	68.7	56.5	82.2	84.2	92.6
FreqNet	99.6	100.0	93.4	98.6	88.0	99.5	90.5	96.0	90.2	99.7	95.8	99.6	85.7	99.8	88.9	94.4	48.0	49.6	71.9	80.1	85.2	91.4
NPR	99.9	100.0	80.9	83.0	99.6	100.0	84.0	85.6	98.1	99.8	95.2	98.1	99.8	100.0	77.2	76.0	60.6	62.9	64.4	66.0	<u>85.9</u>	87.1
ours	99.9	100.0	86.3	97.4	99.9	100.0	87.1	93.6	99.9	100.0	97.1	98.9	90.8	95.9	64.5	72.2	77.8	87.9	65.6	70.6	86.9	<u>91.7</u>

Table 1: Cross-GAN-Sources Evaluation on the test set of ForenSynths [Wang *et al.*, 2020]. **Bold** and underline represent the best and second-best performance, respectively.

Method	BEGAN		SNGAN		CramerGAN		MMDGAN		RelGAN		STGAN		S3GAN		AttGAN		InfoMaxGAN		Mean	
	Acc.	A.P.	Acc.	A.P.	Acc.	A.P.	Acc.	A.P.	Acc.	A.P.	Acc.	A.P.	Acc.	A.P.	Acc.	A.P.	Acc.	A.P.	Acc.	A.P.
CNNDetection	50.2	44.9	62.7	90.4	81.5	97.5	72.9	94.4	53.3	82.1	63.0	92.7	55.2	66.1	51.1	83.7	71.1	94.7	62.3	82.9
Patchfor	97.1	100.0	97.6	99.8	97.8	99.9	97.9	100.0	99.6	100.0	92.7	99.8	66.8	68.8	68.0	92.9	93.6	98.6	90.1	95.4
F3Net	87.1	97.5	51.6	93.6	89.5	99.8	73.7	99.6	98.8	100.0	60.3	99.9	65.4	70.0	85.2	94.8	67.1	83.1	75.4	93.1
GANDetection	67.9	100.0	66.7	90.6	67.8	99.7	67.7	99.3	60.9	86.2	69.6	97.2	69.6	83.5	57.4	75.1	67.6	92.4	66.1	91.6
LGrad	69.9	89.2	78.0	87.4	50.3	50.3	57.5	67.3	89.1	99.1	54.8	68.0	78.5	86.0	68.6	93.8	71.1	82.0	68.6	80.8
Ojha	88.9	96.3	87.7	96.5	89.8	99.1	89.7	99.0	94.0	98.1	82.6	91.5	94.7	98.9	90.0	96.8	87.4	96.5	89.4	97.0
FreqNet	98.8	100.0	85.4	90.4	95.2	98.2	95.2	98.2	100.0	100.0	98.8	100.0	88.3	94.3	89.8	98.8	94.0	97.5	94.0	97.5
NPR	99.6	99.9	93.3	97.3	98.5	98.3	98.5	98.3	99.8	100.0	99.6	100.0	79.8	78.9	92.5	98.6	91.5	97.2	<u>94.8</u>	<u>96.5</u>
ours	97.7	99.8	96.4	99.6	98.2	99.8	98.8	99.9	98.8	88.8	99.4	100.0	83.4	90.2	98.7	99.8	96.8	99.7	96.5	98.7

Table 2: Cross-GAN-Sources Evaluation on the 9 GANs dataset [Tan *et al.*, 2024a].

Method	DDPM		VQ-Diffusion		SDv1		ADM		SDv2		IDDPM		PNDM		LDM		Mean	
	Acc.	A.P.	Acc.	A.P.	Acc.	A.P.	Acc.	A.P.	Acc.	A.P.	Acc.	A.P.	Acc.	A.P.	Acc.	A.P.	Acc.	A.P.
CNNDetection	62.7	76.6	50.0	71.0	38.0	76.7	53.9	71.8	52.0	90.3	50.2	82.7	50.8	90.3	50.4	78.7	51.0	90.3
Patchfor	62.3	97.1	100.0	100.0	90.7	99.8	77.5	93.9	94.8	100.0	50.0	91.6	50.2	99.9	99.5	100.0	78.1	97.8
F3Net	84.7	99.4	100.0	100.0	73.4	97.2	80.9	96.9	99.8	100.0	74.7	98.9	72.8	99.5	100.0	100.0	85.8	99.0
GANDetection	62.3	46.4	51.1	51.2	39.8	65.6	51.1	53.1	50.1	36.9	50.2	63.0	50.6	79.0	51.6	48.1	50.8	55.4
LGrad	99.9	100.0	96.2	100.0	90.4	99.4	86.4	97.5	97.1	100.0	66.1	92.8	69.5	98.5	99.7	100.0	88.2	98.5
Ojha	72.9	78.8	77.7	99.2	59.0	93.0	88.7	98.6	53.3	87.6	73.4	97.1	86.2	99.2	50.7	87.9	70.2	92.5
FreqNet	91.4	99.8	100.0	100.0	63.9	98.1	67.2	91.3	81.8	98.4	59.0	97.3	85.2	99.8	98.9	100.0	80.9	98.1
NPR	99.4	100.0	100.0	100.0	97.3	99.8	88.7	98.6	96.4	100.0	87.5	98.3	97.5	100.0	100.0	100.0	<u>95.8</u>	<u>99.6</u>
ours	99.4	100.0	99.9	100.0	95.6	99.7	96.3	99.4	99.2	100.0	99.4	100.0	99.4	100.0	99.8	100.0	98.7	99.9

Table 3: Cross-Diffusion-Sources Evaluation on the test of DiffusionForensics [Wang *et al.*, 2023].

Method	Guided		Glide_50_27		Glide_100_10		Glide_100_27		LDM_100		LDM_200		LDM_200_cfg		dalle		Mean	
	Acc.	A.P.	Acc.	A.P.	Acc.	A.P.	Acc.	A.P.	Acc.	A.P.	Acc.	A.P.	Acc.	A.P.	Acc.	A.P.	Acc.	A.P.
CNNDetection	54.9	66.6	54.2	76.0	53.3	72.9	53.0	71.3	51.9	63.7	52.0	64.5	51.6	63.1	51.8	61.3	52.8	67.4
Patchfor	74.2	81.4	84.9	98.8	87.3	99.7	82.8	99.1	95.8	99.8	95.6	99.9	94.0	99.8	79.8	99.1	86.8	97.2
F3Net	69.2	70.8	88.5	95.4	88.3	95.4	87.0	94.5	74.1	84.0	73.4	83.3	80.7	89.1	71.6	79.9	79.1	86.5
GANDetection	50.1	51.0	51.7	53.5	51.2	52.6	51.1	51.9	54.7	65.8	54.9	65.9	53.8	58.9	67.2	83.0	54.3	60.1
LGrad	71.8	76.0	91.6	96.0	90.9	95.5	88.5	94.2	95.7	99.3	94.7	99.1	95.1	99.0	89.9	97.8	89.8	94.6
Ojha	69.7	87.6	79.1	99.8	77.9	94.5	78.5	95.3	95.0	99.3	99.0	99.3	74.0	92.5	87.3	97.5	82.6	95.7
FreqNet	67.3	75.7	86.7	96.3	87.9	96.4	84.5	96.0	97.9	99.9	97.5	99.9	97.4	99.9	97.4	99.8	89.6	95.5
NPR	74.8	78.8	98.3	99.8	98.7	99.7	98.2	99.8	98.8	99.8	99.0	99.8	98.8	99.7	95.9	99.7	<u>94.8</u>	<u>97.0</u>
ours	82.4	87.1	98.3	99.7	97.6	99.8	97.6	99.6	99.4	100.0	99.3	100.0	99.0	99.9	86.0	95.6	95.0	97.7

Table 4: Cross-Diffusion-Sources Evaluation on the diffusion test set of Ojha [Ojha *et al.*, 2023].

4.5 Ablation Study

To thoroughly evaluate the effectiveness of each component in our method, we conduct ablation experiments by systematically removing some of the proposed modules. The re-

sults of these experiments, shown in Table 7, demonstrate the contribution of each module to deepfake detection. Notably, when we remove our main module (LoSFB), the performance of our method drops significantly, falling below 50%. This

Method	ADM		Glide		Midjourney		SDv1.4		SDv1.5		VQDM		Wukong		DALI2		Mean	
	Acc.	A.P.	Acc.	A.P.	Acc.	A.P.	Acc.	A.P.	Acc.	A.P.	Acc.	A.P.	Acc.	A.P.	Acc.	A.P.	Acc.	A.P.
LGrad	65.8	70.2	60.6	73.8	64.6	70.3	65.9	68.7	66.3	69.1	67.2	70.6	63.2	65.0	66.9	86.9	65.1	71.8
Ojha	67.6	87.2	61.7	85.5	56.7	74.5	63.1	87.2	62.8	86.3	84.9	96.8	71.2	90.9	49.5	60.2	73.5	83.6
FreqNet	83.3	91.5	81.7	88.9	69.9	79.0	64.3	74.3	64.9	75.5	81.7	89.6	57.7	67.0	55.1	54.6	69.8	77.6
NPR	70.6	75.1	77.2	83.2	76.6	82.6	76.8	82.8	78.0	83.8	75.2	77.7	74.5	78.2	61.9	71.6	73.9	79.4
ours	80.2	83.7	80.8	93.0	73.0	79.4	78.4	84.1	77.8	87.9	83.2	88.7	75.5	78.0	71.3	89.6	77.6	85.6

Table 5: Cross-Diffusion-Sources Evaluation on the GenImage Dataset [Zhu *et al.*, 2024].

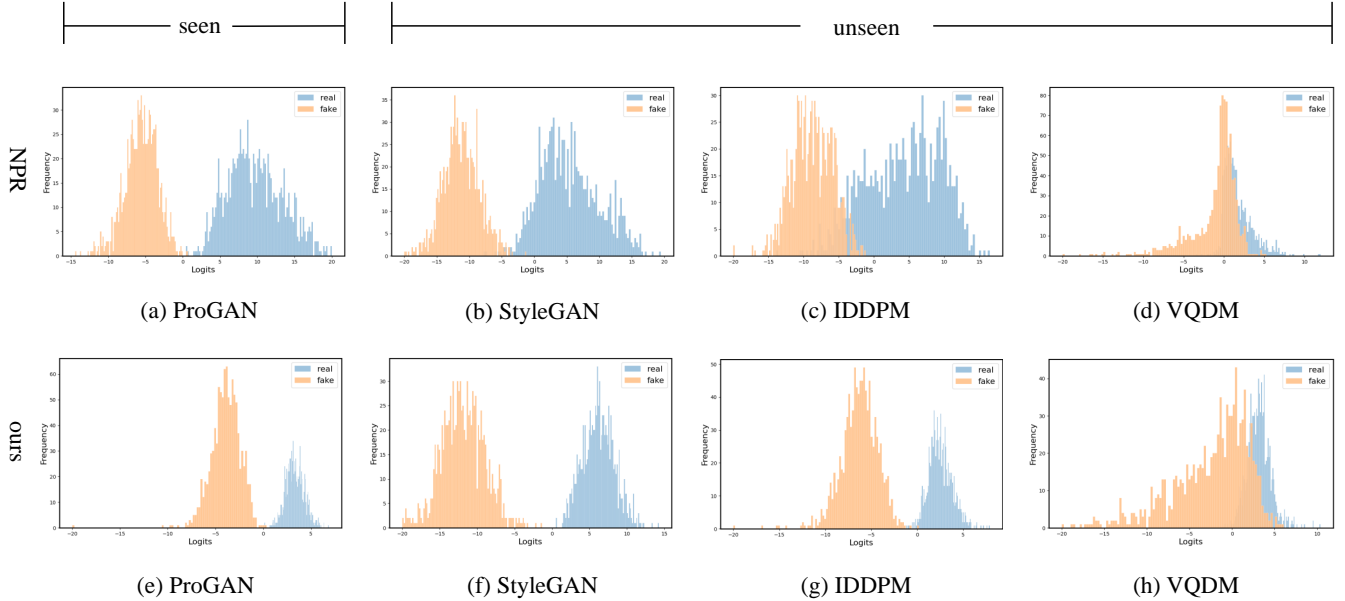


Figure 4: **Logit Distributions of Extracted Forgery Features.** We compare the state of the art NPR [Tan *et al.*, 2024b] and our method, both tuned with 4-class ProGAN [Karras, 2017] data. A total of four testing GANs and diffusion models are considered, including ProGAN [Karras, 2017], StyleGAN [Karras, 2019], IDDPM [Nichol and Dhariwal, 2021] and VQDM [Gu *et al.*, 2022], each randomly sampled 1k real and 1k fake images.

Method	Mean Acc. of 16 sub-testsets
CNNDetection[Wang <i>et al.</i> , 2020]	70.8
LGrad[Tan <i>et al.</i> , 2023]	75.3
Ojha[Ojha <i>et al.</i> , 2023]	78.4
FreqNet[Tan <i>et al.</i> , 2024a]	78.1
NPR[Tan <i>et al.</i> , 2024b]	<u>81.8</u>
ours	84.7

Table 6: The mean accuracy of all 16 generation models on GenImage [Zhu *et al.*, 2024] dataset.

DWT	Window Tiling	FFT	WAttention	mean Acc.	mean A.P.
			✓	67.2	70.8
		✓	✓	49.5	52.3
✓	✓		✓	82.3	87.6
✓		✓	✓	83.9	90.2
✓	✓	✓	✓	84.7	90.9

Table 7: Ablation study on the GenImage [Zhu *et al.*, 2024].

highlights the crucial role of local spatial-frequency domain feature extraction in detecting forged information. To further validate the effectiveness and rationale behind using the phase component of FFT to extract global information and employing sliding window tiling for local feature extraction in DWT, we remove these modules individually. As shown in the table, the accuracy decreased by 2.4% and 0.8%, respectively. These results emphasize the importance of both effectively extracting local texture information and subtle forged textures embedded in the global information.

5 Conclusion

In this paper, we propose a novel and effective method for deepfake detection, leveraging both local spatial-frequency information and global frequency domain features through two core modules: LoSFB and GloFB. This plug-and-play feature extractor is meticulously designed to capture a broader and more effective set of artifact features. Extensive experiments on 34 diverse generative models strongly demonstrate the generalization capability of our method.

6 Acknowledgments

This work is supported by the National Key R&D Program of China under grant 2021YFB2700900; by the National Natural Science Foundation of China under grant U22B2062, 62172232; by the Jiangsu Basic Research Programs-Natural Science Foundation under grant numbers BK20200039; by the Collaborative Innovation Center of Atmospheric Environment and Equipment Technology (CICAET) fund.

References

- [Brock, 2018] Andrew Brock. Large scale gan training for high fidelity natural image synthesis. *arXiv preprint arXiv:1809.11096*, 2018.
- [Chai *et al.*, 2020] Lucy Chai, David Bau, Ser-Nam Lim, and Phillip Isola. What makes fake images detectable? understanding properties that generalize. In *Computer Vision–ECCV 2020: 16th European Conference, Glasgow, UK, August 23–28, 2020, Proceedings, Part XXVI 16*, pages 103–120. Springer, 2020.
- [Chen and Yang, 2020] Zehao Chen and Hua Yang. Manipulated face detector: Joint spatial and frequency domain attention network. *arXiv preprint arXiv:2005.02958*, 1(2):4, 2020.
- [Chen *et al.*, 2021] Shen Chen, Taiping Yao, Yang Chen, Shouhong Ding, Jilin Li, and Rongrong Ji. Local relation learning for face forgery detection. In *Proceedings of the AAAI conference on artificial intelligence*, volume 35, pages 1081–1088, 2021.
- [Chen *et al.*, 2022] Liang Chen, Yong Zhang, Yibing Song, Lingqiao Liu, and Jue Wang. Self-supervised learning of adversarial example: Towards good generalizations for deepfake detection. In *Proceedings of the IEEE/CVF conference on computer vision and pattern recognition*, pages 18710–18719, 2022.
- [Choi *et al.*, 2018] Yunjey Choi, Minje Choi, Munyoung Kim, Jung-Woo Ha, Sunghun Kim, and Jaegul Choo. StarGAN: Unified generative adversarial networks for multi-domain image-to-image translation. In *Proceedings of the IEEE conference on computer vision and pattern recognition*, pages 8789–8797, 2018.
- [Dai *et al.*, 2019] Tao Dai, Jianrui Cai, Yongbing Zhang, Shu-Tao Xia, and Lei Zhang. Second-order attention network for single image super-resolution. In *Proceedings of the IEEE/CVF conference on computer vision and pattern recognition*, pages 11065–11074, 2019.
- [Dhariwal and Nichol, 2021] Prafulla Dhariwal and Alexander Nichol. Diffusion models beat gans on image synthesis. *Advances in neural information processing systems*, 34:8780–8794, 2021.
- [Gu *et al.*, 2022] Shuyang Gu, Dong Chen, Jianmin Bao, Fang Wen, Bo Zhang, Dongdong Chen, Lu Yuan, and Baining Guo. Vector quantized diffusion model for text-to-image synthesis. In *Proceedings of the IEEE/CVF conference on computer vision and pattern recognition*, pages 10696–10706, 2022.
- [Haliassos *et al.*, 2021] Alexandros Haliassos, Konstantinos Vougioukas, Stavros Petridis, and Maja Pantic. Lips don’t lie: A generalisable and robust approach to face forgery detection. In *Proceedings of the IEEE/CVF conference on computer vision and pattern recognition*, pages 5039–5049, 2021.
- [Ho *et al.*, 2020] Jonathan Ho, Ajay Jain, and Pieter Abbeel. Denoising diffusion probabilistic models. *Advances in neural information processing systems*, 33:6840–6851, 2020.
- [Jeong *et al.*, 2022] Yonghyun Jeong, Doyeon Kim, Youngmin Ro, and Jongwon Choi. Freggan: robust deepfake detection using frequency-level perturbations. In *Proceedings of the AAAI conference on artificial intelligence*, volume 36, pages 1060–1068, 2022.
- [Karras *et al.*, 2020] Tero Karras, Samuli Laine, Miika Aittala, Janne Hellsten, Jaakko Lehtinen, and Timo Aila. Analyzing and improving the image quality of stylegan. In *Proceedings of the IEEE/CVF conference on computer vision and pattern recognition*, pages 8110–8119, 2020.
- [Karras, 2017] Tero Karras. Progressive growing of gans for improved quality, stability, and variation. *arXiv preprint arXiv:1710.10196*, 2017.
- [Karras, 2019] Tero Karras. A style-based generator architecture for generative adversarial networks. *arXiv preprint arXiv:1812.04948*, 2019.
- [Kingma, 2014] Diederik P Kingma. Adam: A method for stochastic optimization. *arXiv preprint arXiv:1412.6980*, 2014.
- [Lei Ba *et al.*, 2016] Jimmy Lei Ba, Jamie Ryan Kiros, and Geoffrey E Hinton. Layer normalization. *ArXiv e-prints*, pages arXiv-1607, 2016.
- [Liu *et al.*, 2020] Zhengzhe Liu, Xiaojuan Qi, and Philip HS Torr. Global texture enhancement for fake face detection in the wild. In *Proceedings of the IEEE/CVF conference on computer vision and pattern recognition*, pages 8060–8069, 2020.
- [Liu *et al.*, 2022] Luping Liu, Yi Ren, Zhijie Lin, and Zhou Zhao. Pseudo numerical methods for diffusion models on manifolds. *arXiv preprint arXiv:2202.09778*, 2022.
- [Mandelli *et al.*, 2022] Sara Mandelli, Nicolò Bonettini, Paolo Bestagini, and Stefano Tubaro. Detecting gan-generated images by orthogonal training of multiple cnns. In *2022 IEEE International Conference on Image Processing (ICIP)*, pages 3091–3095. IEEE, 2022.
- [Mao *et al.*, 2024] Xintian Mao, Jiansheng Wang, Xingran Xie, Qingli Li, and Yan Wang. Loformer: Local frequency transformer for image deblurring. In *Proceedings of the 32nd ACM International Conference on Multimedia*, pages 10382–10391, 2024.
- [Nichol and Dhariwal, 2021] Alexander Quinn Nichol and Prafulla Dhariwal. Improved denoising diffusion probabilistic models. In *International conference on machine learning*, pages 8162–8171. PMLR, 2021.

- [Nichol *et al.*, 2021] Alex Nichol, Prafulla Dhariwal, Aditya Ramesh, Pranav Shyam, Pamela Mishkin, Bob McGrew, Ilya Sutskever, and Mark Chen. Glide: Towards photorealistic image generation and editing with text-guided diffusion models. *arXiv preprint arXiv:2112.10741*, 2021.
- [Ojha *et al.*, 2023] Utkarsh Ojha, Yuheng Li, and Yong Jae Lee. Towards universal fake image detectors that generalize across generative models. In *Proceedings of the IEEE/CVF Conference on Computer Vision and Pattern Recognition*, pages 24480–24489, 2023.
- [Park *et al.*, 2019] Taesung Park, Ming-Yu Liu, Ting-Chun Wang, and Jun-Yan Zhu. Semantic image synthesis with spatially-adaptive normalization. In *Proceedings of the IEEE/CVF conference on computer vision and pattern recognition*, pages 2337–2346, 2019.
- [Qian *et al.*, 2020] Yuyang Qian, Guojun Yin, Lu Sheng, Zixuan Chen, and Jing Shao. Thinking in frequency: Face forgery detection by mining frequency-aware clues. In *European conference on computer vision*, pages 86–103. Springer, 2020.
- [Ramesh *et al.*, 2021] Aditya Ramesh, Mikhail Pavlov, Gabriel Goh, Scott Gray, Chelsea Voss, Alec Radford, Mark Chen, and Ilya Sutskever. Zero-shot text-to-image generation. In *International conference on machine learning*, pages 8821–8831. Pmlr, 2021.
- [Rombach *et al.*, 2022] Robin Rombach, Andreas Blattmann, Dominik Lorenz, Patrick Esser, and Björn Ommer. High-resolution image synthesis with latent diffusion models. In *Proceedings of the IEEE/CVF conference on computer vision and pattern recognition*, pages 10684–10695, 2022.
- [Rossler *et al.*, 2019] Andreas Rossler, Davide Cozzolino, Luisa Verdoliva, Christian Riess, Justus Thies, and Matthias Nießner. Faceforensics++: Learning to detect manipulated facial images. In *Proceedings of the IEEE/CVF international conference on computer vision*, pages 1–11, 2019.
- [Russakovsky *et al.*, 2015] Olga Russakovsky, Jia Deng, Hao Su, Jonathan Krause, Sanjeev Satheesh, Sean Ma, Zhiheng Huang, Andrej Karpathy, Aditya Khosla, Michael Bernstein, et al. Imagenet large scale visual recognition challenge. *International journal of computer vision*, 115:211–252, 2015.
- [Schuhmann *et al.*, 2021] Christoph Schuhmann, Richard Vencu, Romain Beaumont, Robert Kaczmarczyk, Clayton Mullis, Aarush Katta, Theo Coombes, Jenia Jitsev, and Aran Komatsuzaki. Laion-400m: Open dataset of clip-filtered 400 million image-text pairs. *arXiv preprint arXiv:2111.02114*, 2021.
- [Tan *et al.*, 2023] Chuangchuang Tan, Yao Zhao, Shikui Wei, Guanghua Gu, and Yunchao Wei. Learning on gradients: Generalized artifacts representation for gan-generated images detection. In *Proceedings of the IEEE/CVF Conference on Computer Vision and Pattern Recognition*, pages 12105–12114, 2023.
- [Tan *et al.*, 2024a] Chuangchuang Tan, Yao Zhao, Shikui Wei, Guanghua Gu, Ping Liu, and Yunchao Wei. Frequency-aware deepfake detection: Improving generalizability through frequency space domain learning. In *Proceedings of the AAAI Conference on Artificial Intelligence*, volume 38, pages 5052–5060, 2024.
- [Tan *et al.*, 2024b] Chuangchuang Tan, Yao Zhao, Shikui Wei, Guanghua Gu, Ping Liu, and Yunchao Wei. Rethinking the up-sampling operations in cnn-based generative network for generalizable deepfake detection. In *Proceedings of the IEEE/CVF Conference on Computer Vision and Pattern Recognition*, pages 28130–28139, 2024.
- [Wang *et al.*, 2020] Sheng-Yu Wang, Oliver Wang, Richard Zhang, Andrew Owens, and Alexei A Efros. Cnn-generated images are surprisingly easy to spot... for now. In *Proceedings of the IEEE/CVF conference on computer vision and pattern recognition*, pages 8695–8704, 2020.
- [Wang *et al.*, 2023] Zhendong Wang, Jianmin Bao, Wengang Zhou, Weilun Wang, Hezhen Hu, Hong Chen, and Houqiang Li. Dire for diffusion-generated image detection. In *Proceedings of the IEEE/CVF International Conference on Computer Vision*, pages 22445–22455, 2023.
- [Wu *et al.*, 2024] Jiahui Wu, Yu Zhu, Xiaoben Jiang, Yatong Liu, and Jiajun Lin. Local attention and long-distance interaction of rppg for deepfake detection. *The Visual Computer*, 40(2):1083–1094, 2024.
- [Xue *et al.*, 2023] Ziyu Xue, Xiuhua Jiang, Qingtong Liu, and Zhaoshan Wei. Global-local facial fusion based gan generated fake face detection. *Sensors*, 23(2):616, 2023.
- [Yu *et al.*, 2015] Fisher Yu, Ari Seff, Yinda Zhang, Shuran Song, Thomas Funkhouser, and Jianxiong Xiao. Lsun: Construction of a large-scale image dataset using deep learning with humans in the loop. *arXiv preprint arXiv:1506.03365*, 2015.
- [Yu *et al.*, 2019] Ning Yu, Larry S Davis, and Mario Fritz. Attributing fake images to gans: Learning and analyzing gan fingerprints. In *Proceedings of the IEEE/CVF international conference on computer vision*, pages 7556–7566, 2019.
- [Yu *et al.*, 2020] Yang Yu, Rongrong Ni, and Yao Zhao. Mining generalized features for detecting ai-manipulated fake faces. *arXiv preprint arXiv:2010.14129*, 2020.
- [Zhao *et al.*, 2021] Hanqing Zhao, Wenbo Zhou, Dongdong Chen, Tianyi Wei, Weiming Zhang, and Nenghai Yu. Multi-attentional deepfake detection. In *Proceedings of the IEEE/CVF conference on computer vision and pattern recognition*, pages 2185–2194, 2021.
- [Zhao *et al.*, 2024] Chen Zhao, Weiling Cai, Chenyu Dong, and Chengwei Hu. Wavelet-based fourier information interaction with frequency diffusion adjustment for underwater image restoration. In *Proceedings of the IEEE/CVF Conference on Computer Vision and Pattern Recognition*, pages 8281–8291, 2024.
- [Zhu *et al.*, 2017] Jun-Yan Zhu, Taesung Park, Phillip Isola, and Alexei A Efros. Unpaired image-to-image translation

using cycle-consistent adversarial networks. In *Proceedings of the IEEE international conference on computer vision*, pages 2223–2232, 2017.

[Zhu *et al.*, 2024] Mingjian Zhu, Hanting Chen, Qiangyu Yan, Xudong Huang, Guanyu Lin, Wei Li, Zhijun Tu, Hailin Hu, Jie Hu, and Yunhe Wang. Genimage: A million-scale benchmark for detecting ai-generated image. *Advances in Neural Information Processing Systems*, 36, 2024.